JACS
JOURNAL OF THE AMERICAN CHEMICAL SOCIETY
Article
pubs.acs.org/JACS

# Rigidifying Fluorescent Linkers by Metal–Organic Framework Formation for Fluorescence Blue Shift and Quantum Yield Enhancement

Zhangwen Wei,[†,∥] Zhi-Yuan Gu,[†,∥] Ravi K. Arvapally,[§,∥] Ying-Pin Chen,[†,‡] Roy N. McDougald, Jr.,[§] Joshua F. Ivy,[§] Andrey A. Yakovenko,[†] Dawei Feng,[†] Mohammad A. Omary,*[,§] and Hong-Cai Zhou*[,†,‡]

[†]Department of Chemistry, Texas A&M University, College Station, Texas 77843, United States
[‡]Department of Materials Science and Engineering, Texas A&M University, College Station, Texas 77842, United States
[§]Department of Chemistry, University of North Texas, Box 305070, Denton, Texas 76203-5070, United States

Supporting Information

**ABSTRACT:** We demonstrate that rigidifying the structure of fluorescent linkers by structurally constraining them in metal–organic frameworks (MOFs) to control their conformation effectively tunes the fluorescence energy and enhances the quantum yield. Thus, a new tetraphenylethylene-based zirconium MOF exhibits a deep-blue fluorescent emission at 470 nm with a unity quantum yield (99.9 ± 0.5%) under Ar, representing ca. 3600 $cm^{-1}$ blue shift and doubled radiative decay efficiency vs the linker precursor. An anomalous increase in the fluorescence lifetime and relative intensity takes place upon heating the solid MOF from cryogenic to ambient temperatures. The origin of these unusual photoluminescence properties is attributed to twisted linker conformation, intramolecular hindrance, and framework rigidity.

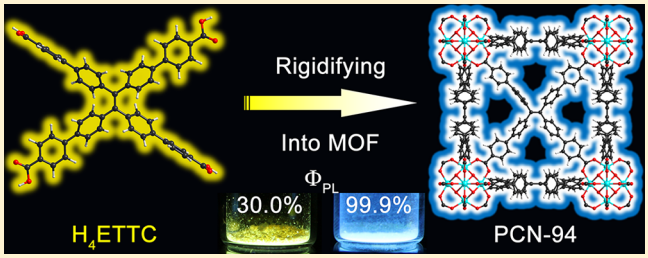


## INTRODUCTION

Fluorescent solid materials have attracted significant attention because of their wide applications especially as inorganic and organic light-emitting diodes (LEDs and OLEDs, respectively) and solid state sensors.[1] Discovering new fluorescent materials with intriguing properties, such as stimuli responsiveness and high porosity, will facilitate the development of functional materials enriching the current inorganic and organic solid semiconductors. Despite the large diversity of small organic fluorescent molecules, which provide almost infinite potential candidates for fluorescent and phosphorescent solids, these materials usually suffer from self-quenching and the consequent low quantum yield of their photo- or electroluminescence.[2] Recently, it has been shown that it is possible to turn on the fluorescence by building the fluorophore within metal–organic frameworks (MOFs).[3] Herein we propose a MOF with rigidified fluorescent linkers to effectively tune the frontier orbital energy gap (or semiconductor band gap) and improve the photoluminescence quantum yield, dramatically to attain unity.

MOFs, constructed from inorganic metal-containing nodes and organic linkers bearing large internal surface areas, diverse structures, and versatile functionalities,[2,4] can be promising candidates as tunable OLED emitters and luminescent sensors. Their luminescence originates from metal cations, most commonly lanthanides, the organic linkers, or charge transfers between the two.[2,5]

Rigidifying linkers in MOFs has two distinctive advantages. First, the linkers can adopt some special conformations that would otherwise be impossible, hence producing different fluorescence and/or absorption energies. Second, the linkers fixed in the porous frameworks have longer intermolecular separations and, as a result, can increase photoluminescence quantum yield due to decreased self-quenching. It will be of great scientific and technological significance to show a proof-of-concept demonstration that rigidifying fluorescent linkers by MOF formation would efficiently and substantially tune the electronic transition energies and raise the quantum yields.

As a conventional fluorophore, tetraphenylethylene (TPE), Figure 1a, is well-known for its aggregation-induced emission (AIE) character.[6] Nevertheless, only several pioneering papers have discussed the utilization of TPE in MOFs to turn-on its fluorescence.[3] On the other hand, further applications of reported TPE-based MOFs are limited due to their moisture-sensitivity originating from the labile coordination bonds between divalent metal cations and carboxylate linkers.

Here we undertake a combined structural/spectroscopic study of a new extended TPE-based linker and a robust tetravalent zirconium MOF thereof (PCN-94, where PCN stands for "porous coordination network") that exhibits remarkably high fluorescence quantum yield in the solid state, among other unusual photophysical properties. We designed

**Received:** January 22, 2014
**Published:** May 12, 2014




dx.doi.org/10.1021/ja5006866 | J. Am. Chem. Soc. 2014, 136, 8269–8276

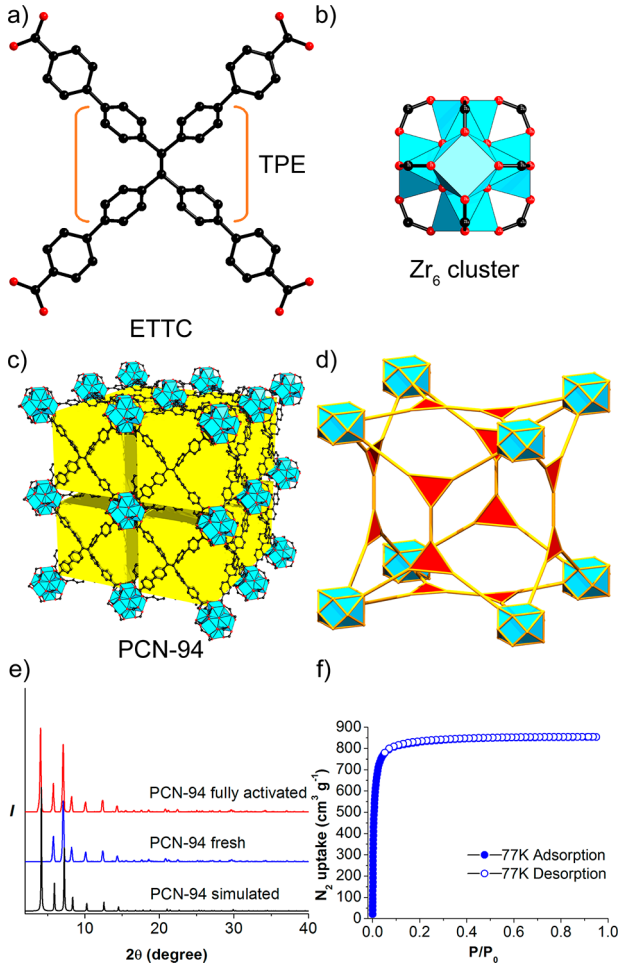


**Figure 1.** (a-d) Crystal structure views of PCN-94 showing: (a) ETTC in PCN-94; orange brackets indicate the TPE core; (b) $Zr_6$ cluster; (c) PCN-94 framework; (d) topological representation of PCN-94. All H atoms are omitted, and only one orientation of the disordered atoms is shown for clarity. Color scheme: black, C; red, O; blue polyhedron, Zr; yellow cube, cavity with 17.5 Å edge. (e) PXRD patterns of PCN-94; (f) $N_2$ uptake of PCN-94 under 77 K and 1 atm.

and synthesized a tetracarboxylate linker precursor, 4′,4‴,4⁗,4⁗′-(ethene-1,1,2,2-tetrayl)tetrakis(([1,1′-biphenyl]-4-carboxylic acid)), henceforth denoted as "$H_4$ETTC", and crystallized it with Zr(IV); see Figure 1a and Figure S1 (in Supporting Information, SI). Given the loss of the 5s and 4d electrons in Zr(IV), the resulting closed-shell electronic configuration is employed for building fluorescent MOFs that preclude paramagnetic quenching by the metal center[7] yet maintain the extraordinary chemical and thermal stability known for Zr-MOFs.[8] Rigidifying the yellow-emitting TPE-based organic linker, ETTC, into PCN-94 produced ultrabright blue fluorescence with a quantum yield as high as 99.9 ± 0.5% under inert atmosphere and room temperature. This rigidifying methodology provided a promising approach for the development of deep-blue emitters with high fluorescence quantum yield, which are highly coveted in white OLEDs for solid-state lighting or video display applications.[1d,e]

## EXPERIMENTAL SECTION

**General Information.** The commercial chemicals are used as purchased unless otherwise mentioned. Detailed chemical sources are provided in the SI.

The electronic absorption spectra were measured on a Hitachi U-4100 UV−vis−NIR spectrophotometer. Steady-state luminescence spectra were acquired with a PTI QuantaMaster Model QM-4 scanning spectrofluorometer equipped with a 75-W xenon lamp, emission and excitation monochromators, excitation correction unit, and a PMT detector. The excitation and emission spectra have been corrected for the wavelength-dependent lamp intensity and detector response, respectively. Lifetime data were acquired using a nitrogen laser interfaced with a tunable dye laser and a frequency doubler, as part of fluorescence and phosphorescence subsystem add-ons to the PTI instrument. The 337.1 nm line of the $N_2$ laser was used either directly or to pump a freshly prepared $1 \times 10^{-2}$ M solution of an organic continuum laser dye such as Coumarin-540A in ethanol, the output of which was tuned and frequency doubled to attain the appropriate excitation used to generate the time-resolved data. All the lifetime measurements for PCN-94 were performed with $\lambda_{em}/\lambda_{exc}$ = 445/400 nm, while the lifetime measurements for $H_4$ETTC were performed with $\lambda_{em}/\lambda_{exc}$ = 535/400 nm. Temperature-dependent studies were acquired with an Oxford optical cryostat using liquid nitrogen as the coolant. Quantum yields were measured with an integration sphere coupled to the PTI spectrofluorometer. All the quantum yield measurements for PCN-94 were performed with $\lambda_{exc}$ = 375 nm, while the quantum yield measurements for $H_4$ETTC were performed with $\lambda_{exc}$ = 420 nm. Elemental analyses (C, H) were obtained on a PerkinElmer 240 elemental analyzer. Thermogravimetry analysis (TGA) was conducted on a TGA-50 (SHIMADZU) thermogravimetric analyzer. Nuclear magnetic resonance (NMR) data were collected on a Mercury 300 spectrometer. Fourier transform infrared (IR) measurements were performed on a SHIMADU IR Affinity-1 spectrometer. For mass spectrometry, electrospray ionization was performed using an Applied Biosystems QSTAR Pulsar (Concord, ON, Canada). Sample was directly infused at flow rate of 7 μL/min through a 50 μm ID fused-silica capillary. Electrospray needle voltage was held at 4500 V in positive mode and −4500 V in negative mode. Nebulizer and curtain gas flow rates were held at 40 and 20 PSI respectively. X-ray photoelectron spectra (XPS) were acquired with Axis Ultra DlD (Kratos) equipped with Al monochromatic X-rays operating at 12 kV and 10 mA. In situ synchrotron-based powder diffraction experiments were performed at the 17-BM beamline of the Advanced Photon Source in Argonne National Laboratory (Argonne, IL, USA).

**Synthesis of 4′,4‴,4⁗,4⁗′-(Ethene-1,1,2,2-tetrayl)tetrakis(([1,1′-biphenyl]-3-carboxylic acid)) ($H_4$ETTC).** *Tetrakis(4-bromophenyl)ethene.*[9] The experiment detail is provided in SI.

*Tetramethyl 4′,4‴,4⁗,4⁗′-(ethene-1,1,2,2-tetrayl)tetrakis([1,1′-biphenyl]-4-carboxylate).* Tetrakis(4-bromophenyl)ethene (1.5 g, 0.0023 mol, 1.0 equiv), 4-methoxycarbonylphenylboronic acid (2.5 g, 0.014 mol, 6.1 equiv), cesium fluoride (4.2 g, 0.028 mol, 12.2 equiv) and tetrakis(triphenylphosphine)palladium (0.2 g, 0.0002 mol, 0.09 equiv) were added to a 250 mL three-neck round-bottom flask charged with a stir bar. Degassed dimethoxyethane (150 mL) was transferred to the system, and the solution was refluxed for 48 h. After the reaction mixture was cooled to room temperature, the solvent was evaporated, and the solid was dissolved in dichloromethane and washed with water. The organic phase was separated and dried with magnesium sulfate. After removal of the solvent with a rotary evaporator, the solid was recrystallized from acetone to yield a light yellow product (1.6 g, 0.018 mol, 80% yield based on tetrakis(4-bromophenyl)ethene): $^1$H NMR (300 MHz, $CDCl_3$) $\delta$ 3.93 (s, 12H), 7.19 (d, 8H), 7.44 (d, 8H), 7.62 (d, 8H), 8.05(d, 8H); $^{13}$C NMR (300 MHz, $CDCl_3$) $\delta$ 52.26, 126.80, 126.86, 128.96, 130.19, 132.16, 138.18, 140.72, 143.53, 144.95, 167.05; FTIR (neat) 2947 (w), 2562 (w), 2068 (w), 1929 (w), 1721 (s), 1605 (m), 1435 (w), 1273 (s), 1188 (m), 1103 (s), 1003 (m), 833 (s), 771 (s), 702 (s), 648 (w) cm$^{-1}$; Mass spectrum calcd 863.3, found 875.3 (+Li). Anal. Calcd (%): C, 80.17; H, 5.10. Found: C, 79.48; H, 5.10.

*4′,4‴,4⁗,4⁗′-(Ethene-1,1,2,2-tetrayl)tetrakis(([1,1′-biphenyl]-4-carboxylic acid)) ($H_4$ETTC).* Tetramethyl 4′,4‴,4⁗,4⁗′-(ethene-1,1,2,2-tetrayl)tetrakis([1,1′-biphenyl]-4-carboxylate) (1.6 g, 0.0018 mol, 1.0 equiv) and sodium hydroxide (1.7 g, 0.0425 mol, 23.6 equiv)


dx.doi.org/10.1021/ja5006866 | J. Am. Chem. Soc. 2014, 136, 8269−8276

were added into a mixture of tetrahydrofuran (THF), methanol, and water (150 mL, v/v/v = 1:1:1). The mixture was refluxed overnight. After removal of the organic layer, the aqueous phase was acidified with HCl (6 M) to yield a yellow precipitate of 4′,4‴,4⁗,4⁗′-(ethene-1,1,2,2-tetrayl)tetrakis(([1,1′-biphenyl]-3-carboxylic acid)) ($H_4$ETTC), which was filtered, washed with water, and dried under vacuum. Yield 1.4 g (0.0018 mol, 95%, based on the ester): $^1$H NMR (300 MHz, DMSO-$d_6$) $\delta$ 7.19 (d, 8H), 7.61 (d, 8H), 7.76 (d, 8H), 7.95 (d, 8H); $^{13}$C NMR (300 MHz, DMSO-$d_6$) $\delta$, 126.59, 129.64, 130.04, 131.71, 137.12, 140.30, 143.14, 143.44, 167.20; FTIR (neat) 3032 (w), 2484 (w), 1690 (s), 1605 (s), 1389 (m), 1250 (s), 1186 (m), 1121 (m), 991 (m), 900 (w), 758 (s), 705 (m) cm$^{-1}$; Mass spectrum calcd 812.2, found 811.1 (+H). Anal. Calcd (%): C, 79.79; H, 4.46. Found: C, 79.41; H, 4.78.

The single crystal of $H_4$ETTC for X-ray diffraction study was obtained by evaporating its *N*,*N*-dimethylformamide solution.

**Synthesis of PCN-94.** In a 4 mL Pyrex vial, $ZrCl_4$ (30 mg, 0.13 mmol, 7.2 equiv), $H_4$ETTC (15 mg, 0.018 mmol, 1.0 equiv) and benzoic acid (260 mg, 2.1 mmol, 1166 equiv) were ultrasonically dissolved in *N*,*N*-diethylformamide (DEF, 1.8 mL). The mixture was heated in an oven kept at 120 °C for 24 h. After cooling to room temperature, colorless cubic single crystals suitable for X-ray structure determination were obtained.

In a 4 mL Pyrex vial, $ZrCl_4$ (30 mg, 0.13 mmol, 7.2 equiv), $H_4$ETTC (15 mg, 0.018 mmol, 1.0 equiv) and acetic acid (0.2 mL) were ultrasonically dissolved in *N*,*N*-dimethylformamide (DMF, 1.8 mL). The mixture was heated in an oven kept at 120 °C for 24 h. After cooling to room temperature, a white powder of pure-phase PCN-94 was obtained for characterization. Anal. Calcd (%): C, 62.65; H, 3.25. Found: C, 61.02; H, 3.41.[10]

**X-ray Crystallography.** Single crystal X-ray crystallographic data were collected on a Bruker single-crystal APEXII CCD Diffractometer with Mo K$\alpha$ ($\lambda$ = 0.71073 Å) at 110 K. All structures were solved by direct method and refined by full-matrix least-squares on $F^2$ using *SHELXTL*.[11] Non-hydrogen atoms were refined with anisotropic displacement parameters during the final cycles. Organic hydrogen atoms were placed in calculated positions with isotropic displacement parameters set to 1.2 × $U_{eq}$ of the attached atom. The solvent molecules are highly disordered, and attempts to locate and refine the solvent peaks were unsuccessful. Contributions to scattering due to these solvent molecules were removed using the *SQUEEZE* routine of *PLATON*;[12] structures were then refined again using the data generated. Crystal data are summarized in Table 1. The CIF file can be obtained free of charge from the Cambridge Crystallographic Data Centre via www.ccdc.cam.ac.uk/data_request/cif (CCDC 951017 for PCN-94, 991702 for $H_4$ETTC).

The powder X-ray diffraction patterns (PXRD) were recorded on a BRUKER D8-Focus Bragg–Brentano X-ray Powder Diffractometer equipped with a Cu sealed tube ($\lambda$ = 1.54178 Å) at room temperature. The simulated PXRD spectra were obtained by the diffraction-crystal module of the *Mercury* program based on the single-crystal data. The program is available free of charge via the Internet at http:/www.iucr.org.

For in situ PXRD measurements, powdery samples were soaked in acetone and sucked into a 0.9 mm diameter polyimide capillary by a syringe. The capillary was installed on a flow cell equipped with gas-load tubing and a temperature controller. PXRD patterns were collected at the 17-BM beamline of the Advanced Photon Source in Argonne National Laboratory (Argonne, IL, USA). The incident beam wavelength was 0.72910 Å for the experiments performed from 50 to 473 °C, and 0.72959 Å for the experiments performed from 298 to 100 K. Data were gathered angularly from 1° to 25° in 2$\theta$ with a step interval of 0.015° using a Perkin-Elmer flat panel area detector (XRD 1621 CN3-EHS) at various temperatures under a He atmosphere. The raw images were processed within Fit-2D program, refining the sample-to-detector distance and tilt of the detector relative to the beam based on $LaB_6$ standard.

**Gas Adsorption Measurements.** Gas adsorption–desorption isotherms were measured using a Micromeritics ASAP2020 system with ultra high purity (UHP) grade gases. After cooling to room temperature, as-synthesized PCN-94 (~100 mg) sample was washed twice with DMF and acetone, respectively. Fresh acetone was subsequently added, and the sample was allowed to stay for 24 h to exchange and remove the nonvolatile solvates (DMF). After removal of acetone by decanting, the sample was activated by drying under vacuum overnight, and it was dried again by using the "outgas" function of the adsorption instrument for 10 h at 120 °C prior to gas adsorption/desorption measurements.

**Density Functional Theory (DFT) Computations.** The computations were performed with the DFTB+ and DMol3 programs of Materials Studio 6.0.[13] The resultant energy data of calculated structures are listed in Table 2. Frequency calculations were carried out and analyzed to assess whether the optimized structures represent the true minima.

**Table 1. Crystal Data for PCN-94 and $H_4$ETTC**

| formula | $C_{162}H_{96}O_{32}Zr_6$ | $C_{72}H_{78}N_6O_{14}$ |
|---|---|---|
| $F_w$ | 3101.71 | 1251.40 |
| color/shape | colorless/cube | colorless/block |
| crystal size (mm$^3$) | 0.30 × 0.25 × 0.20 | 0.30 × 0.20 × 0.10 |
| crystal system | cubic | orthorhombic |
| space group | *Pm*3*m* | *Fdd*2 |
| *a*, *b*, *c* (Å) | 21.104(3) | 20.558(6), 78.02(2), 8.621(2) |
| $\alpha$, $\beta$, $\gamma$ (deg) | 90 | 90 |
| *V* (Å$^3$) | 9399.1(19) | 13847(6) |
| *Z* | 1 | 8 |
| $d_{calc}$ (g/cm$^3$) | 0.548 | 1.201 |
| $\mu$ (mm$^{-1}$) | 0.189 | 0.084 |
| *T* (K) | 110(2) | 110(2) |
| *F*(000) | 1564 | 5312 |
| reflns collected | 98 813 | 30 987 |
| independent reflns | 1867 | 5676 |
| obsd data [$I > 2\sigma(I)$] | 1634 | 3248 |
| data/restraints/parameters | 1867/19/28 | 5676/22/313 |
| completeness | 99.4% | 99.7% |
| GOF on $F_2$ | 1.006 | 1.004 |
| $R_{int}$ | 0.1513 | 0.1032 |
| $R_1$, $wR_2$ [$I > 2\sigma(I)$] | 0.1188, 0.2496 | 0.1346, 0.2929 |
| $R_1$, $wR_2$ (all data) | 0.1352, 0.2605 | 0.1806, 0.3114 |
| $\Delta\rho_{max}/\Delta\rho_{min}$ [e·Å$^{-3}$] | 1.579/−0.890 | 0.585/−0.505 |

**Table 2. Computational Results of $H_4$ETTC in Twisted and Free Conformation**

| | $H_4$ETTC in twisted conformation | $H_4$ETTC in free conformation |
|---|---|---|
| total energy (kcal mol$^{-1}$) | −1680963.3 | −1681163.3 |
| zero point vibrational energy (kcal mol$^{-1}$) | 464.4 | 467.4 |
| first vibrational frequency (cm$^{-1}$) | – | 4.8 |

The twisted conformation of $H_4$ETTC was obtained by changing four Zr cations to protons and removing other Zr cations connected to the ETTC unit in PCN-94. The molecule was optimized through the DFTB+ program by fixing all C and O atoms and relaxing only the H atoms. The usage of twisted conformation has been justified by comparing with two other conformations (Section S5 (SI): DFT Calculations).

The $H_4$ETTC in free conformation was relaxed with DFTB+ from $H_4$ETTC in the PCN-94 conformation. DMol3 optimization using the PBE functional and DNP 4.4 basis file was performed to attain the final $H_4$ETTC structure in free conformation.


dx.doi.org/10.1021/ja5006866 | *J. Am. Chem. Soc.* 2014, 136, 8269–8276

The HOMO, LUMO, and simulated UV−vis spectra were obtained with the DMol3 energy calculation using PBE and DNP 4.4 basis files.

## RESULTS AND DISCUSSION

**Rigidifying the TPE-Based Linkers by MOF Formation.** PCN-94 crystallizes in space group *Pm*3*m* with $a$ = 21.104(3) Å (Table 1). Each ETTC (crystallographically disordered) unit connects to four $Zr_6$ clusters (Figures 1, S10 and S11 (SI)). Every $Zr_6$ cluster links 18 other $Zr_6$ clusters through 12 ETTCs. The framework contains only one type of cubic cages having ca. 17.5 Å edges, with eight $Zr_6$ clusters occupying the vertices and six ETTC moieties covering the faces. Such cavities are packed in a primitive cubic lattice (Figure 1c). Along the [1 1 0] direction are windows with size of 14 × 14 $Å^2$ connecting the cubic cavities (Figure S12a (SI)). From the topological viewpoint, $Zr_6$ cluster serves as a 12-connected node and ETTC as a 3,3-connected nodes. Then PCN-94 adopts a rare 3,3,3,12-c 4 nodal net (Figure 1d) with stoichiometry $(3\text{-c})_2(3\text{-c})_2(3\text{-c})_2(12\text{-c})$ and topological point symbol of $\{4.5^2\}_2\{4.6^2\}_4\{4^{14}.5^8.6^{14}.7^{16}.8^{14}\}$, which is previously unreported. If the ETTC is further simplified as a 4-connected node, the structure of PCN-94 can be simplified as a 4,12-c 2-nodal net with **ftw** topology and the topological point symbol is denoted as $\{4^{36};6^{30}\}\{4^4;6^2\}_3$ (Figure S12b (SI)). Similar **ftw** structures with non-TPE linkers were reported in MOF-525 and MOF-535.[14]

The purity of PCN-94 was examined by PXRD after drying the sample under vacuum at room temperature (Figure 1e). In situ PXRD confirmed that PCN-94 can retain its framework crystallinity until 473 °C under a helium atmosphere (Figure S15 (SI)). TGA curves show that the decomposition temperature is around 430 °C for a fresh PCN-94 sample and 450 °C for the activated sample under a nitrogen atmosphere (Figure S36). Low-temperature in situ PXRD measurements of PCN-94 from 100 to 298 K showed that changes of diffraction peaks are negligible under various temperatures, indicating the preservation of the highly rigid MOF structure (Figure S16 (SI)). An as-synthesized PCN-94 sample was subject to an activation process of solvent exchange with acetone, followed by heating under vacuum. The porosity of the activated sample was evaluated through nitrogen adsorption/desorption studies under 77 K (Figure 1f). The resulting Brunauer−Emmett−Teller (BET) and Langmuir surface areas are 3377 and 3732 $m^2\ g^{-1}$, respectively (Figures S25 and S26 (SI)).[15] The total pore volume is 1.32 $cm^3\ g^{-1}$, matching the value of 1.32 $cm^3\ g^{-1}$ calculated using the *PLATON* routine with a 1.8 Å probe size, indicating that the sample was fully activated.[12] Argon adsorption measurements showed a higher BET surface area of 3757 $m^2\ g^{-1}$ (Figures S27−S29 (SI)). The gas adsorption properties of PCN-94 were evaluated using hydrogen, carbon dioxide and methane (Figures S30−S35 (SI)).

**Photophysical Properties of PCN-94.** To investigate the solid-state absorption and photoluminescence properties, the diffuse reflectance as well as the solid-state photoluminescence spectra of PCN-94 and its linker precursor $H_4$ETTC were measured (Figure 2a). The diffuse reflectance spectrum shows that $H_4$ETTC has a broad absorption profile extending between 250 and 600 nm with two discernible features, whereas PCN-94 exhibits significantly sharper absorption ranging from 250 to 500 nm, which is clearly blue-shifted compared to the $H_4$ETTC absorption. Thus, PCN-94 and $H_4$ETTC show distinct colors: $H_4$ETTC is a bright yellow powder owing to absorbing blue

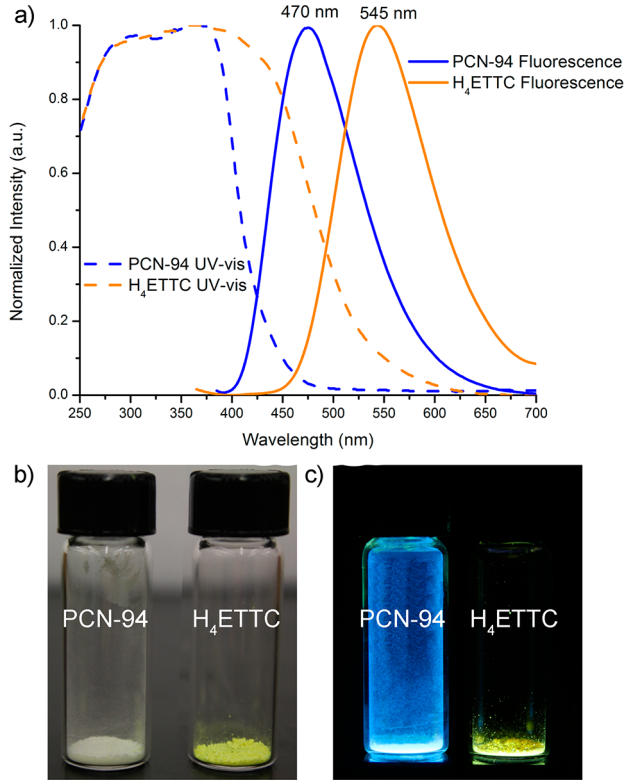


**Figure 2.** (a) Solid-state absorption (via diffuse reflectance; dash lines) and emission spectra (solid lines) of PCN-94 (blue) and $H_4$ETTC (orange) at room temperature (RT). Photos of PCN-94 and $H_4$ETTC are shown under (b) ambient light and (c) UV light.

light while PCN-94 is white with slight discoloration because of only absorbing UV light but reflecting all visible light (Figure 2b). The shorter-wavelength absorption feature and the onset of the overlap from the second longer-wavelength feature nearly coincide for the two materials, whereas the second band for the $H_4$ETTC linker precursor, but not the MOF chromophore, extends to the visible region, consistent with self-aggregation of the ligand.

Solid-state photoluminescence (PL) measurements show that the emission maxima of PCN-94 and $H_4$ETTC are at 470 and 545 nm, respectively (Figure 2a). The emission color shifts to blue in PCN-94 from the yellow emission of $H_4$ETTC (Figure 2c). Moreover, the PL quantum yield (Φ) is 76% for PCN-94 in the solid state at room temperature under ambient atmosphere and increases to 91% upon $N_2$ deaeration (Table 3). This Φ value is extremely high for PCN-94 compared to all reported fluorescent MOFs, including other TPE-core based MOFs.[3] Figure 3 shows the normalized absolute Φ of $H_4$ETTC solid, PCN-94 solid, and the standard reference material quinine sulfate in 1 N sulfuric acid/ethanol solution, for which we obtained 55%, reproducing the reported value, to validate the direct Φ methodology followed in this work.[16] The PL quantum yield becomes essentially unity (within experimental error) upon purging with Ar instead of $N_2$ gas. Independent experiments were reproduced multiple times with long deaeration times (1−1.5 h) to show successive increase in PL intensity, initially by 26.1% under $N_2$ atmosphere (vs 19.7% with short, 10−15 min, deaeration) and then by 4% upon another long purging period under Ar atmosphere. These PL intensity increases give rise to Φ values of 96 and 100% with the experimental errors shown in Table 3 upon sufficiently long


dx.doi.org/10.1021/ja5006866 | J. Am. Chem. Soc. 2014, 136, 8269−8276

**Table 3. Photophysical Parameters for PCN-94 and $H_4$ETTC Solids under Various Conditions**

| | PCN-94 | $H_4$ETTC |
|---|---|---|
| PL quantum yield (%) | 76.2 ± 3.5 (air; RT) | 30.0 ± 0.5 (air; RT) |
| | 91.3 ± 0.5 ($N_2$; RT[a]) 96.1 ± 0.5 ($N_2$; RT[b]) 99.9 ± 0.6 (Ar; RT[b]) | |
| lifetime (ns) | 2.06 ± 0.02 ($N_2$; RT) | $\tau_1$ = 24.74 ± 0.28 |
| | | $\tau_2$ = 4.15 ± 0.07 ($N_2$; RT) |
| | 1.57 ± 0.01 ($N_2$; 70 K) | $\tau_1$ = 31.54 ± 0.55 |
| | | $\tau_2$ = 4.87 ± 0.19 ($N_2$; 90 K) |
| | 1.83 ± 0.02 ($N_2$; 140 K) | |
| | 1.87 ± 0.02 ($N_2$; 250 K) | |

[a]Short (10−15 min) purging time. [b]Long (1−1.5 h) purging time.

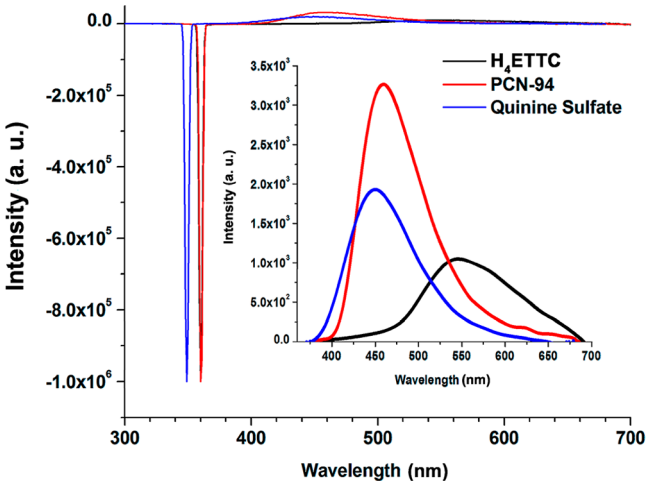


**Figure 3.** A plot of the emission spectra used for the absolute quantum yield determination of PCN-94, $H_4$ETTC solids and quinine sulfate solution. The spectra are normalized for the absorption signal at the excitation wavelength used for each sample. The inset shows the expanded portion of the emission scanned within 380−700 nm.

deaeration conditions under $N_2$ and Ar atmospheres, respectively. While typical fluorescent materials do not undergo as significant $O_2$ quenching as phosphorescent materials do (due to the spin-forbidden energy transfer from the former to the triplet ground state of $O_2$), the fact that PCN-94 is a porous material renders the quenching by $O_2$ and other potential impurity quenchers present in ambient air (e.g., $CO_2$ and $H_2O$) more facile than the situation for a nonporous fluorophore.

The high quantum yield of PCN-94 is primarily attributed to the immobilization of the ETTC linker as it is strongly coordinated to Zr(IV), and to the diminution of concentration quenching that is very common for luminescent organic molecules.[17] The formation of a rigid MOF via coordination of the ETTC to the Zr(IV) cation prevents the torsional relaxation, which is the general deactivation pathway for substituted tetraphenylethylenes.[18] The longer component ($\tau_1$) of the PL lifetime of $H_4$ETTC is almost an order of magnitude slower than that of PCN-94, whereas the shorter component ($\tau_2$) is only a factor of 2 slower within the same order of magnitude (Table 3). The order-of-magnitude slower decay of $\tau_1$ is expected and well-documented for excimeric emissions in fluorescent materials.[19] On the other hand, the faster decay of the ETTC fluorophore within PCN-94 is because the pertinent aromatic units are highly twisted, and are constrained as such via the coordination to the Zr(IV) centers. Consequently, their structural rigidity prevents their excited-state distortion, hence the exciton immediately releases the energy via fluorescence and results in a shorter lifetime. On the other hand, the chromophores in $H_4$ETTC exist in a low-energy free conformation that allows for free rotation around the C−C single bonds between the aromatic rings, which leads to a more facile excited-state distortion and slower emission decay from individual ETTC units ($\tau_2$) in comparison to the monoexponential decay in PCN-94. While the solid state suppresses this excited-state distortion to an extent, resulting in a significant quantum yield of ∼30% for solid $H_4$ETTC, the suppression is even higher and the distortion is essentially prevented in PCN-94, resulting in a unity quantum yield. The excimer route upon intermolecular association of ETTC rings in $H_4$ETTC leads to yet greater deceleration, hence much longer PL lifetimes for the $\tau_1$ component by an order of magnitude, as the process requires significant compression of the interplanar distances between the aromatic rings of multiple $H_4$ETTC molecules. Neither the intermolecular nor the intramolecular excited state distortion is allowed in PCN-94 due to the coordination chemistry involved that "freezes" the ETTC fluorophoric units in a twisted conformation, resulting in a remarkably fast radiative decay ($k_r$ = 4.85−6.37 × $10^8$ $s^{-1}$) and unity quantum yield. The emission decay of PCN-94 is monoexponential with a fluorescence lifetime of 2.06 ns at RT, whereas $H_4$ETTC exhibits a biexponential fluorescence decay. The dual $H_4$ETTC lifetimes likely originate from monomer and excimer combination with the latter stemming from phenyl ring interactions in adjacent $H_4$ETTC molecules, which is excimeric in nature (Figure S38 (SI)).

Apart from the high quantum yield of PCN-94, an anomalous fluorescence behavior related to temperature is observed. Generally, as temperature is increased from cryogenic to ambient temperatures, the fluorescence intensity is expected to decrease for most fluorescent materials owing to thermal quenching via multiphoton relaxation pathways. This general behavior is, indeed, observed for $H_4$ETTC (Figure S29 (SI)). For PCN-94, however, increasing the temperature from 70 K toward 298 K results in fluorescence intensity that exhibits an ascending nature (Figure 4a), which also holds true for the corresponding lifetimes (Table 3). This seemingly indicates a paradoxical decrease in the nonradiative fluorescence pathways as temperature increases. Aromatic rings would contract at lower temperatures to increase self-quenching and result in lower fluorescence intensity. Since $\pi$-stacking interaction does not exist in PCN-94, it is ruled out as a possible cause for such an uncommon behavior. A more reasonable explanation is thermal assistance of the $S_2$−$S_1$ internal conversion that supplements the direct excitation route to $S_1$. The spectral profiles of the diffuse reflectance and excitation spectra support such a dual excitation pathway. For $H_4$ETTC, on the other hand, the biexponential decay comes from different excitation routes of the monomer and dimer/excimer species, each with its characteristic decay independently as discussed above based on the time-resolved data (Figures S44 and S45 (SI)). Figure 4b substantiates the hypothesis that the broadened, red-shifted fluorescence peak observed for solid $H_4$ETTC likely stems from an excimeric species, as a peak at a nearly identical peak maximum appears in the nearly saturated (1 × $10^{-3}$ M) solution in THF while a more dilute (1 × $10^{-5}$ M) solution exhibited a blue-shifted peak maximum by ca. 1200 $cm^{-1}$,


dx.doi.org/10.1021/ja5006866 | J. Am. Chem. Soc. 2014, 136, 8269−8276

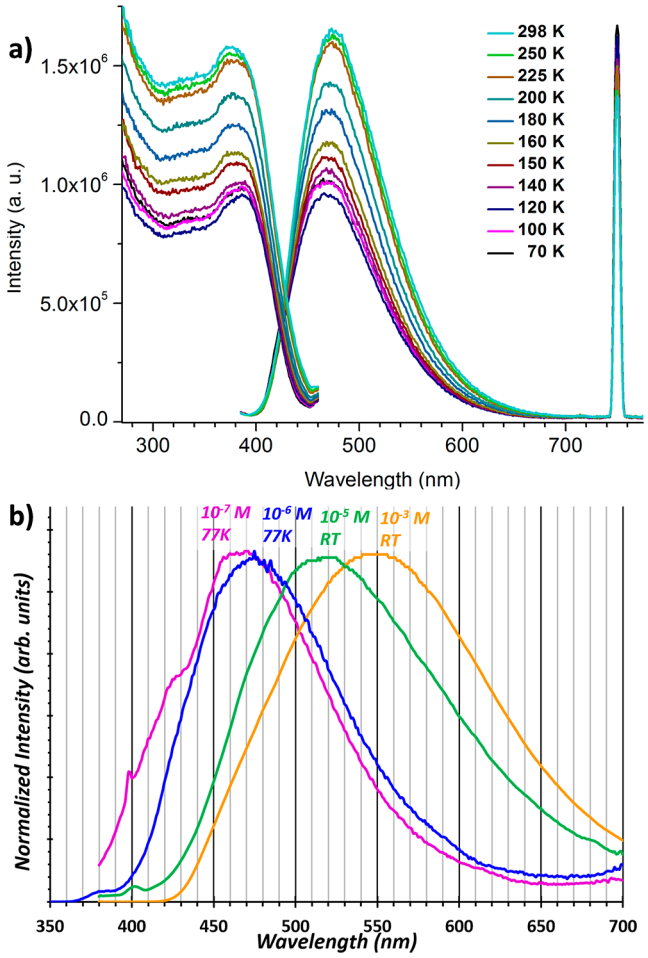


**Figure 4.** (a) Temperature dependent steady state fluorescence excitation (left) and emission (right) spectra for PCN-94. $\lambda_{exc}$ = 375 nm and $\lambda_{em}$ = 470 nm. The second harmonic peak is shown to validate relative fluorescence intensity at different temperature. (b) Concentration-dependent fluorescence spectra of $H_4$ETTC in THF solution, suggesting aggregation at high concentration akin to the solid-state spectrum of $H_4$ETTC in Figure 2a.

whereas additional dilution ($1 \times 10^{-6}$ M) did not attain further blue shift and the signal-to-noise ratio was rather small. To enhance the detectability, the fluorescence spectra for such dilute solutions were acquired at 77 K for a glassy matrix. Only under such conditions for infinitesimally dilute $H_4$ETTC (0.1–1.0 $\mu$M) did the chromophore approach the emission range of solid PCN-94! The 0.1 $\mu$M frozen glass of $H_4$ETTC attains a monomer-like structured fluorescence under such conditions that favor higher PL spectral resolution. Remarkably, the solid-state complexation of the ETTC chromophore to Zr(IV) in PCN-94 inhibits the intermolecular (and intramolecular) interactions and/or excited-state distortion modes of fluorophore moieties more so than infinitesimal dilution in solution under ambient conditions! This is evidenced by the greater blue shift exceeding 3000 $cm^{-1}$ in the porous solid MOF vs the $1 \times 10^{-3}$ M solution and by ca. 1800 $cm^{-1}$ vs the $1 \times 10^{-5}$ M or $1 \times 10^{-6}$ M solutions. Figure 5 summarizes the qualitative models for the photophysical pathways that account for the PCN-94 and $H_4$ETTC fluorescence bands.

On the basis of the peak profile, lifetime, and energy, the emission is described as linker-centered fluorescence. The hypsochromic shift of PCN-94 comparing to $H_4$ETTC suggests

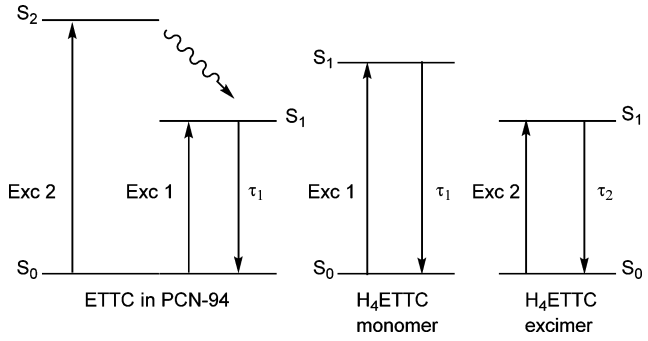


**Figure 5.** Schematic representation of the electronic transition levels of ETTC in PCN-94 and $H_4$ETTC.

an increase in the HOMO–LUMO energy gap of the ETTC moiety. XPS experiment confirmed that the PCN-94 contains Zr(IV) (Figure S37 (SI)).[20] This blue shift is originally attributed to ligand-field stabilization of the filled $\pi$ levels and/or destabilization of the vacant $\pi^*$ of the $ETTC^{4-}$ linker upon coordination to Zr(IV) in PCN-94. The high-valence Zr(IV) cation has a closed-shell configuration with all the 5s and 4d valence orbitals empty. These orbitals could overlap with the ligand $\pi$ orbitals and extend the delocalized conjugate system, leading to red-shifted emission.[7] However, we obtain the opposite result. In this case, we propose that the conjugation is not extended to the Zr(IV) metal center in the emissive excited state, which is largely localized on the ETTC moiety. The lack of vibronic structure in the spectral profile even at cryogenic temperatures (Figure 4a) is likely due to the $\pi$-system conjugation involving eight aromatic rings and an unsaturated C=C bond, although we cannot completely rule out partial metal participation in the emissive state. The next section offers more insights on spectral shifts upon rigidified conformation.

**Rigidifying Mechanism and Molecular Simulations.** Unlike the free conformation of $H_4$ETTC, a prominent conformational change was observed for the twisted ETTC linker in PCN-94, where the minimum angle between adjacent carboxylate groups of ETTC became enlarged from ca. 65° to 86° (Figures 7 and S13 (SI)). The average dihedral angles between the phenyl rings (<P2–P3) as well as between phenyl rings and the central plane of ETTC (<P1–P2) in PCN-94 are much larger than those in the free conformation (Figures 6 and S22 (SI); Table 4). The larger dihedral angles result in less efficient overlap of the p orbitals of all the $sp^2$-hybridized C

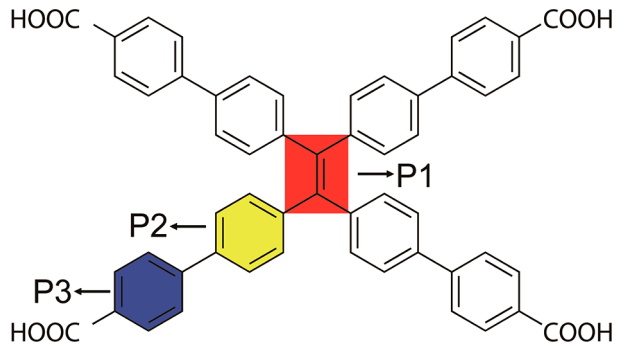


**Figure 6.** Plane definitions within the structure of ETTC: Red plane P1 is defined by the two C atoms forming the central C=C double bond and four C atoms surround them. The yellow and blue phenyl rings define the P2 and P3 plane crossing them, respectively.


dx.doi.org/10.1021/ja5006866 | J. Am. Chem. Soc. 2014, 136, 8269–8276

**Table 4. Average Dihedral Angles[a] of $H_4$ETTC in the PCN-94 Conformation and in Free Conformation**

| | in PCN-94 conformation | in free conformation |
|---|---|---|
| P1−P2 (deg) | 55.33 | 50.20 |
| P2−P3 (deg) | 54.45 | 35.93 |

[a]Refer to Figure 6 for the definition of P1, P2, and P3.

atoms. Thus, the delocalized conjugate system of the linker breaks down, leading to a widened energy gap between HOMO and LUMO. This breakdown of the conjugate system is mainly responsible for the large blue-shift of the electronic absorption and emission bands. To clearly and quantitatively demonstrate the mechanism, DFT calculations were performed on both the free and twisted $H_4$ETTC (Figure 7), ignoring the minor

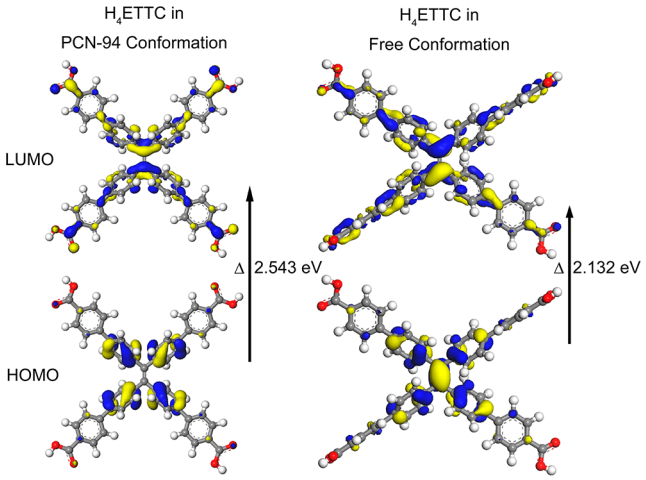


**Figure 7.** Contour plots of the HOMO and LUMO for $H_4$ETTC in PCN-94 conformation and in free conformation, respectively.

difference between $H_4ETTC^{4-}$ and ETTC twisted to the same extent. The results indicate that the energy gap between the HOMO and LUMO is widened from 2.132 to 2.543 eV, which should lead to higher excitation and emission energies in the latter. Indeed, the simulated UV−vis spectra (TD-DFT simulations) of $H_4$ETTC in the twisted conformation shows absorption bands between 400 and 500 nm, whereas the free conformation covers longer wavelengths up to 550 nm (Figure S23 (SI)). The blue-shifted UV−vis absorption bands for the twisted conformation in these simulated spectra are in agreement with the experimental results. The twisted conformation of ETTC produces a widened energy gap, thus producing not only largely blue-shifted UV−vis absorption bands, but also blue-shifted fluorescence bands. The single crystal structure of $H_4$ETTC has also been determined, showing a conformation similar to the simulated one for the linker precursor, validating the results of the DFT computations.

Rigidifying linkers also contributes to the quantum yield increase. Fixation of twisted ETTC by the MOF formation separates every ETTC moiety from each other, decreasing interlinker interactions. In addition, the repulsion between H atoms on adjacent phenyl rings of ETTC decreases the thermal motion of phenyl rings and intralinker interactions (Figure S14 (SI)). Both factors effectively eliminate the thermal motions of ETTC atoms, making the excited linker release the extra energy through fluorescence and substantially increasing the quantum yield.[3c]

## CONCLUSIONS

We have demonstrated that the fluorescence energy and quantum yield of fluorophores can be tuned by rigidifying them as linkers of metal−organic framework. A highly fluorescent MOF, PCN-94, composed of a TPE-core linker and a $Zr_6$ cluster, was synthesized. The twisted linker conformation in PCN-94 induced bright-blue fluorescence emission at 470 nm, which is hypsochromically shifted from the 545 nm yellow emission of linker precursor $H_4$ETTC. The quantum yield of PCN-94 is as high as unity (99.9 ± 0.5%), which comes from the reduced intra- and intermolecular interactions. This work has demonstrated a rare example that linker conformation can produce significant effects on photophysical properties of MOFs, which represents a new strategy to attain light-emitting MOFs that may be suitable for potential applications in molecular electronics and/or sensor technologies.

## ASSOCIATED CONTENT

### Supporting Information

Materials, material synthesis, in situ powder X-ray diffraction patterns, additional structure figures, DFT calculation details, additional adsorption isotherms and BET statistics, and crystal data (CIF). This material is available free of charge via the Internet at http://pubs.acs.org.

## AUTHOR INFORMATION

### Corresponding Author

zhou@mail.chem.tamu.edu; omary@unt.edu

### Author Contributions

[‖]Z.W., Z.-Y.G., and R.K.A. contributed equally.

### Notes

The authors declare no competing financial interest.

## ACKNOWLEDGMENTS

This work was supported as part of the Center for Gas Separations Relevant to Clean Energy Technologies, an Energy Frontier Research Center (EFRC) funded by the U.S. Department of Energy (DOE), Office of Science, Office of Basic Energy Sciences under Award Number DE-SC0001015, and part of the Methane Opportunities for Vehicular Energy (MOVE) Program, an ARPA-E Project under Award Number DE-AR0000249. Z.W. and D.F. were supported by MOVE. Y.-P.C. and Z.-Y.G. were supported by EFRC. M.A.O. acknowledges support of his group's contributions by the National Science Foundation (CHE-0911690; CMMI-0963509; CHE-0840518) and the Robert A. Welch Foundation (Grant B-1542). Use of the Advanced Photon Source, an Office of Science User Facility operated for the U.S. Department of Energy (DOE) Office of Science by Argonne National Laboratory, was supported by the U.S. DOE under Contract No. DE-AC02-06CH11357. Use of the TAMU Materials Characterization Facility and Dr. Amanda Young for helping on some fluorescence and UV−vis spectra measurements, Dr. Jing Wu for XPS measurements are acknowledged. We thank Dr. Yohannes Rezenom of the Laboratory for Biological Mass Spectrometry at Texas A&M University for the assistance in the mass spectrometry analysis. We also thank Dr. Lisa Perez, Zhenggang Xu and Dr. Qian Peng from the Supercomputing Facility at Texas A&M and Laboratory for Molecular

Simulation for offering access to computing time and valuable discussions.

## REFERENCES

(1) (a) Yang, J. S.; Swager, T. M. *J. Am. Chem. Soc.* **1998**, *120*, 11864. (b) Moerner, W. E.; Orrit, M. *Science* **1999**, *283*, 1670. (c) Gunnlaugsson, T.; Glynn, M.; Tocci, G. M.; Kruger, P. E.; Pfeffer, F. M. *Coord. Chem. Rev.* **2006**, *250*, 3094. (d) Baldo, M. A.; O'Brien, D. F.; You, Y.; Shoustikov, A.; Sibley, S.; Thompson, M. E.; Forrest, S. R. *Nature* **1998**, *395*, 151. (e) D'Andrade, B. W.; Forrest, S. R. *Adv. Mater.* **2004**, *16*, 1585.

(2) Cui, Y.; Yue, Y.; Qian, G.; Chen, B. *Chem. Rev.* **2012**, *112*, 1126.

(3) (a) Shustova, N. B.; McCarthy, B. D.; Dincă, M. *J. Am. Chem. Soc.* **2011**, *133*, 20126. (b) Shustova, N. B.; Cozzolino, A. F.; Reineke, S.; Baldo, M.; Dincă, M. *J. Am. Chem. Soc.* **2013**, *135*, 13326. (c) Shustova, N. B.; Ong, T.-C.; Cozzolino, A. F.; Michaelis, V. K.; Griffin, R. G.; Dincă, M. *J. Am. Chem. Soc.* **2012**, *134*, 15061. (d) Shustova, N. B.; Cozzolino, A. F.; Dincă, M. *J. Am. Chem. Soc.* **2012**, *134*, 19596.

(4) (a) Sumida, K.; Rogow, D. L.; Mason, J. A.; McDonald, T. M.; Bloch, E. D.; Herm, Z. R.; Bae, T.-H.; Long, J. R. *Chem. Rev.* **2012**, *112*, 724. (b) Suh, M. P.; Park, H. J.; Prasad, T. K.; Lim, D.-W. *Chem. Rev.* **2012**, *112*, 782. (c) Li, J.-R.; Sculley, J.; Zhou, H.-C. *Chem. Rev.* **2012**, *112*, 869. (d) Wu, H.; Gong, Q.; Olson, D. H.; Li, J. *Chem. Rev.* **2012**, *112*, 836. (e) Ma, S.; Zhou, H.-C. *Chem. Commun.* **2010**, *46*, 44. (f) Makal, T. A.; Li, J.-R.; Lu, W.; Zhou, H.-C. *Chem. Soc. Rev.* **2012**, *41*, 7761. (g) Yoon, M.; Srirambalaji, R.; Kim, K. *Chem. Rev.* **2012**, *112*, 1196. (h) Corma, A.; García, H.; Llabrés i Xamena, F. X. *Chem. Rev.* **2010**, *110*, 4606. (i) Ma, L.; Abney, C.; Lin, W. *Chem. Soc. Rev.* **2009**, *38*, 1248. (j) Farrusseng, D.; Aguado, S.; Pinel, C. *Angew. Chem., Int. Ed.* **2009**, *48*, 7502. (k) Seo, J. S.; Whang, D.; Lee, H.; Jun, S. I.; Oh, J.; Jeon, Y. J.; Kim, K. *Nature* **2000**, *404*, 982. (l) Allendorf, M. D.; Bauer, C. A.; Bhakta, R. K.; Houk, R. J. T. *Chem. Soc. Rev.* **2009**, *38*, 1330. (m) Kreno, L. E.; Leong, K.; Farha, O. K.; Allendorf, M.; Van Duyne, R. P.; Hupp, J. T. *Chem. Rev.* **2012**, *112*, 1105. (n) Jiang, H.-L.; Tatsu, Y.; Lu, Z.-H.; Xu, Q. *J. Am. Chem. Soc.* **2010**, *132*, 5586. (o) Takashima, Y.; Martínez, V. M.; Furukawa, S.; Kondo, M.; Shimomura, S.; Uehara, H.; Nakahama, M.; Sugimoto, K.; Kitagawa, S. *Nat. Commun.* **2011**, *2*, 168. (p) An, J.; Geib, S. J.; Rosi, N. L. *J. Am. Chem. Soc.* **2009**, *131*, 8376. (q) Della Rocca, J.; Liu, D.; Lin, W. *Acc. Chem. Res.* **2011**, *44*, 957. (r) Horcajada, P.; Gref, R.; Baati, T.; Allan, P. K.; Maurin, G.; Couvreur, P.; Férey, G.; Morris, R. E.; Serre, C. *Chem. Rev.* **2012**, *112*, 1232. (s) Zhang, W.; Xiong, R.-G. *Chem. Rev.* **2012**, *112*, 1163. (t) Zhang, J.-P.; Zhang, Y.-B.; Lin, J.-B.; Chen, X.-M. *Chem. Rev.* **2012**, *112*, 1001. (u) Bétard, A. l.; Fischer, R. A. *Chem. Rev.* **2011**, *112*, 1055. (v) Stock, N.; Biswas, S. *Chem. Rev.* **2012**, *112*, 933. (w) O'Keeffe, M.; Yaghi, O. M. *Chem. Rev.* **2012**, *112*, 675. (x) Cook, T. R.; Zheng, Y.-R.; Stang, P. J. *Chem. Rev.* **2013**, *113*, 734. (y) Gagnon, K. J.; Perry, H. P.; Clearfield, A. *Chem. Rev.* **2012**, *112*, 1034. (z) Cohen, S. M. *Chem. Rev.* **2012**, *112*, 970. (aa) Horike, S.; Shimomura, S.; Kitagawa, S. *Nat. Chem.* **2009**, *1*, 695. (ab) Long, J. R.; Yaghi, O. M. *Chem. Soc. Rev.* **2009**, *38*, 1213. (ac) Ferey, G.; Serre, C. *Chem. Soc. Rev.* **2009**, *38*, 1380. (ad) Makal, T. A.; Yakovenko, A. A.; Zhou, H.-C. *J. Phys. Chem. Lett.* **2011**, *2*, 1682. (ae) Zhou, H.-C.; Long, J. R.; Yaghi, O. M. *Chem. Rev.* **2012**, *112*, 673. (af) Yaghi, O. M.; Li, G.; Li, H. *Nature* **1995**, *378*, 703. (ag) Li, H.; Eddaoudi, M.; O'Keeffe, M.; Yaghi, O. M. *Nature* **1999**, *402*, 276. (ah) Kondo, M.; Yoshitomi, T.; Matsuzaka, H.; Kitagawa, S.; Seki, K. *Angew. Chem., Int. Ed.* **1997**, *36*, 1725. (ai) Gu, Z.-Y.; Yang, C.-X.; Chang, N.; Yan, X.-P. *Acc. Chem. Res.* **2012**, *45*, 734.

(5) (a) Zou, J.-P.; Peng, Q.; Wen, Z.; Zeng, G.-S.; Xing, Q.-J.; Guo, G.-C. *Cryst. Growth Des.* **2010**, *10*, 2613. (b) Feng, R.; Jiang, F.-L.; Chen, L.; Yan, C.-F.; Wu, M.-Y.; Hong, M.-C. *Chem. Commun.* **2009**, 5296 DOI: 10.1039/B908792C. (c) Liu, Y.; Pan, M.; Yang, Q.-Y.; Fu, L.; Li, K.; Wei, S.-C.; Su, C.-Y. *Chem. Mater.* **2012**, *24*, 1954. (d) Ablet, A.; Li, S.-M.; Cao, W.; Zheng, X.-J.; Wong, W.-T.; Jin, L.-P. *Chem.—Asian J.* **2013**, *8*, 95. (e) White, K. A.; Chengelis, D. A.; Gogick, K. A.; Stehman, J.; Rosi, N. L.; Petoud, S. p. *J. Am. Chem. Soc.* **2009**, *131*, 18069. (f) Lee, C. Y.; Farha, O. K.; Hong, B. J.; Sarjeant, A. A.; Nguyen, S. T.; Hupp, J. T. *J. Am. Chem. Soc.* **2011**, *133*, 15858. (g) Son, H.-J.; Jin, S.; Patwardhan, S.; Wezenberg, S. J.; Jeong, N. C.; So, M.; Wilmer, C. E.; Sarjeant, A. A.; Schatz, G. C.; Snurr, R. Q.; Farha, O. K.; Wiederrecht, G. P.; Hupp, J. T. *J. Am. Chem. Soc.* **2012**, *135*, 862. (h) Liu, T.-F.; Zhang, W.; Sun, W.-H.; Cao, R. *Inorg. Chem.* **2011**, *50*, 5242.

(6) Vyas, V. S.; Rathore, R. *Chem. Commun.* **2010**, *46*, 1065.

(7) Zhang, W.; Huang, H.; Liu, D.; Yang, Q.; Xiao, Y.; Ma, Q.; Zhong, C. *Microporous Mesoporous Mater.* **2013**, *171*, 118.

(8) (a) Cavka, J. H.; Jakobsen, S.; Olsbye, U.; Guillou, N.; Lamberti, C.; Bordiga, S.; Lillerud, K. P. *J. Am. Chem. Soc.* **2008**, *130*, 13850. (b) Kandiah, M.; Nilsen, M. H.; Usseglio, S.; Jakobsen, S.; Olsbye, U.; Tilset, M.; Larabi, C.; Quadrelli, E. A.; Bonino, F.; Lillerud, K. P. *Chem. Mater.* **2010**, *22*, 6632. (c) Schaate, A.; Roy, P.; Preuße, T.; Lohmeier, S. J.; Godt, A.; Behrens, P. *Chem.—Eur. J.* **2011**, *17*, 9320. (d) Vermoortele, F.; Ameloot, R.; Vimont, A.; Serre, C.; De Vos, D. *Chem. Commun.* **2011**, *47*, 1521. (e) Feng, D.; Gu, Z.-Y.; Li, J.-R.; Jiang, H.-L.; Wei, Z.; Zhou, H.-C. *Angew. Chem., Int. Ed.* **2012**, *51*, 10307. (f) Jiang, H.-L.; Feng, D.; Liu, T.-F.; Li, J.-R.; Zhou, H.-C. *J. Am. Chem. Soc.* **2012**, *134*, 14690. (g) Kim, M.; Cahill, J. F.; Su, Y. X.; Prather, K. A.; Cohen, S. M. *Chem. Sci.* **2012**, *3*, 126.

(9) Vyas, V. S.; Banerjee, M.; Rathore, R. *Tetrahedron Lett.* **2009**, *50*, 6159.

(10) (a) As porous crystalline materials, MOFs are known to trap guest molecules. Hence, it is difficult to fit the EA data. So we provided the calculated elemental content based on the chemical formular of activated sample. (b) Furukawa, H.; Gándara, F.; Zhang, Y.-B.; Jiang, J.; Queen, W. L.; Hudson, M. R.; Yaghi, O. M. *J. Am. Chem. Soc.* **2014**, *136*, 4369.

(11) Sheldrick, G. *Acta Crystallogr., A* **2008**, *64*, 112.

(12) Spek, A. *J. Appl. Crystallogr.* **2003**, *36*, 7.

(13) *Accelerys Materials Studio Release Notes*, Release 5.5.1; Accelrys Software, Inc.: San Diego, 2010.

(14) Morris, W.; Volosskiy, B.; Demir, S.; Gándara, F.; McGrier, P. L.; Furukawa, H.; Cascio, D.; Stoddart, J. F.; Yaghi, O. M. *Inorg. Chem.* **2012**, *51*, 6443.

(15) Walton, K. S.; Snurr, R. Q. *J. Am. Chem. Soc.* **2007**, *129*, 8552.

(16) Melhuish, W. H. *J. Phys. Chem.* **1961**, *65*, 229.

(17) Lacowicz, J. R. *Principles of Fluorescence Spectroscopy*, 2nd ed.; Kluwer Academic/Plenum: New York, 1999.

(18) Ma, J.; Dutt, G. B.; Waldeck, D. H.; Zimmt, M. B. *J. Am. Chem. Soc.* **1994**, *116*, 10619.

(19) Turro, N. J. *Modern Molecular Photochemistry of Organic Molecules*; University Science Books: Sausalito, CA, 2010.

(20) Wagner, C. D.; Riggs, W. M.; Davis, L. E.; Moulder, J. F. *Handbook of X-ray Photoelectron Spectroscopy*; Perkin-Elmer Corp., Eden Prairle, MN, 1979.